JOURNAL OF Materials CHEMISTRY

# Synthesis, characterization and structure determination of Mu-15: a new fluorogallophosphate with fluoride as a specific template of the D4R units

**Alain Matijasic, Jean-Louis Paillaud and Joël Patarin***

*Laboratoire de Matériaux Minéraux, ENSCMu, Université de Haute-Alsace, UPRES-A 7016, 3 rue Alfred Werner, 68093 Mulhouse Cedex, France*

***Received 3rd February 2000, Accepted 22nd March 2000***
***Published on the Web 10th May 2000***

The title compound (Mu-15) is a new three-dimensional fluorinated gallophosphate synthesized from an aqueous fluoride-containing medium, using *N*,*N*,*N*′,*N*′-tetramethyl-1,3-propanediamine (TMP) as organic template. This material was characterized by XRD, SEM, thermal analysis and solid-state NMR spectroscopy ($^{13}C$, $^{19}F$, $^{31}P$, $^{71}Ga$). The structure of Mu-15 ($[Ga_{16}P_{16}O_{60}(OH)_2F_6O_4][H_2TMP]_4$) was determined from XRD powder data. It crystallizes in the space group $Pna2_1$ [$a=16.5779(2)$, $b=9.8223(1)$, $c=13.8562(2)$ Å, $V=2256.25(6)$ Å$^3$] and consists of an arrangement of double-four-ring units (D4R) hosting $F^-$ anions. The connection of these units leads to a three-dimensional but interrupted framework, with two types of channels. The first, parallel to the [100] direction, is delimited by 10-ring apertures, whereas the second channel system, parallel to the [010] direction, is characterized by 8-ring openings. This fluorogallophosphate is another example showing the structure-directing role of $F^-$ towards the D4R units.

## 1 Introduction

Zeolites (*i.e.* aluminosilicate molecular sieves) have been known for a long time.[1] In the eighties, a second family of microporous materials, the metallophosphates, was discovered with the synthesis of the first aluminophosphates.[2] In 1985, the substitution of Al by Ga allowed Parise to prepare several microporous gallophosphates.[3] Since then, a large number of other gallophosphates have been synthesized, particularly by using the fluoride route.[4–6] In this case, fluorine is often present in the material obtained, and generally displays 3 different types of environment. It can be incorporated into the gallophosphate framework bridging two gallium atoms.[7–9] It can also be found as a terminal Ga–F group.[10] Finally, fluoride anions can play a structure-directing role, stabilizing small structural units; the so-called double 4-ring (D4R) units.[4,5,11–14] Table 1 gives a summary of the different gallophosphates presenting such a fluoride environment.

In addition to the fluoride ions, the reaction mixtures involve the presence of an organic template. In particular, the family of diaminoalkanes displays a strong templating role in this system and was extensively used to prepare new gallophosphates.[6,15,16] Thus, ULM-18[6] and Mu-8[16] were synthesized in the presence of *N*,*N*,*N*′,*N*′-tetramethylethylenediamine, whereas, by changing the length of the carbon chain, Weigel and co-workers obtained the gallophosphate TMP–GaPO (TMP = *N*,*N*,*N*′,*N*′-tetramethyl-1,3-propanediamine).[17]

In the present work, we report the synthesis of a new gallophosphate, prepared in a fluoride-containing medium in the presence of the same organic template (TMP). This material, named Mu-15, was characterized by several techniques such as XRD, chemical analysis, SEM, TG/DTA and multi-nuclear solid-state NMR spectroscopy. Its structure determined from XRD powder data is also reported.

## 2 Experimental

### 2.1 Reactants

The reactants were *N*,*N*,*N*′,*N*′-tetramethyl-1,3-propanediamine (TMP, Aldrich, purum >98%), 85% aqueous phosphoric acid ($H_3PO_4$, Prolabo, Normapur) and 40% aqueous hydrofluoric acid (HF, Prolabo, Normapur). The gallium source was an amorphous gallium oxide hydroxide that was prepared by heating a gallium nitrate solution (Rhône-Poulenc) at 250 °C for 24 h.

### 2.2 Synthesis procedure

A pure Mu-15 phase was obtained by hydrothermal synthesis at 130 °C. Typically, the molar composition of the starting gel was: 1 $Ga_2O_3$ : 1 $P_2O_5$ : 1.5 HF : 1 TMP : 80 $H_2O$.

As an example, for sample A (Table 2), the gel was prepared by adding, under stirring, the gallium source (0.28 g) to $H_3PO_4$ (0.29 g) and water (1.7 g). After homogenization, HF (0.09 g) and TMP (0.17 g) were successively introduced. The pH value

**Table 1** Gallophosphates showing $F^-$ anions occluded in the D4R units

| Material or structure type (dimensionality) | Largest ring (no. T atoms) | Reference |
|---|---|---|
| LTA (3D) | 8 | 5 |
| –CLO (3D) | 20 | 4 |
| Mu-1 (molecular anion) | — | 11 |
| Mu-2 (3D) | 8 | 12 |
| Mu-3[a] (1D) | — | 13 |
| Mu-5[a] (3D) | 12 | 14 |
| ULM-5[a] (3D) | 16 | 7 |
| ULM-18 (2D) | — | 6 |

[a]In these fluorogallophosphates, terminal Ga–F groups or Ga–F–Ga bridges are also present.

**Table 2** Syntheses performed in the system $Ga_2O_3$–$P_2O_5$–HF–TMP–$H_2O$ (TMP = *N*,*N*,*N*′,*N*′-tetramethyl-1,3-propanediamine). Starting molar composition: 1 $Ga_2O_3$ : 1 $P_2O_5$ : *x* HF : 1 TMP : 80 $H_2O$

| Sample | HF (*x*) | Heating temperature/°C | Crystallization time/days | XRD results |
|---|---|---|---|---|
| A | 1.5 | 130 | 6 | Mu-15 |
| B | 1.5 | 170 | 3 | Mu-15 + TMP–GaPO[a] |
| C | 3 | 170 | 3 | TMP–GaPO |
| D | 1 | 170 | 3 | $GaPO_4$–C4[24] |
| E | 1 | 130 | 6 | amorphous + Mu-15 |

[a]The underlined phase corresponds to the major phase.

was close to 4. The resulting gel was mixed at room temperature for one hour and transferred into a 20 ml PTFE-lined stainless steel autoclave. The crystallization was carried out at 130 °C under static conditions. After six days of heating, the product was recovered, washed with distilled water and dried at 60 °C overnight.

### 2.3 Thermal analysis

Prior to analysis, the solids were kept in a wet atmosphere over a saturated aqueous solution of $NH_4Cl$ ($P/P_0 = 0.85$) for 24 h to set the hydration state. Thermogravimetric (TGA) and differential thermal (DTA) analyses were performed under air on a Setaram Labsys thermoanalyser with a heating rate of 2 °C $min^{-1}$.

### 2.4 Chemical analysis

Ga and P analysis was performed by inductively coupled plasma emission spectroscopy. $F^-$ content was determined using a fluoride ion-selective electrode after mineralization, and C and N analyses by coulometric and catharometric determinations, respectively, after calcination of the samples.

### 2.5 $^{13}C$, $^{19}F$, $^{31}P$ and $^{71}Ga$ solid-state NMR spectroscopy

The $^{13}C$ CP MAS NMR spectrum was recorded on a Bruker MSL 300, and the $^{19}F$, $^{31}P$ and $^{71}Ga$ NMR spectra on a Bruker DSX 400 spectrometer. The recording conditions of the CP MAS and MAS spectra are given in Table 3.

### 2.6 Powder X-ray diffraction

For the structure determination the XRD powder data were recorded, in Debye–Scherrer geometry, on a STOE STADI-P diffractometer, equipped with a curved germanium(111) primary monochromator and a linear position-sensitive detector (6° 2$\theta$) using Cu-K$\alpha_1$ radiation ($\lambda = 1.5406$ Å). The unit cell parameters were determined applying Werner's trial and error indexing program.[18] The structure analysis was performed using the program package EXPO,[19,20] which integrates EXTRA,[19] a program that extracts structure factor amplitudes by the Le Bail method,[21] and SIRPOW.92,[22] a direct method package especially designed for powder data. The GSAS[23] program was chosen for the Rietveld refinement. For the structure determination the extracted intensities of the reflections up to 60° 2$\theta$ ($d = 1.541$ Å) were taken, while the complete pattern (9–90°) was used for the Rietveld refinement. A summary of the experimental data is given in Table 4.

## 3 Results and discussion

### 3.1 Synthesis and crystal morphology

As can be seen clearly from Table 2, Mu-15 crystallizes in a very narrow range of synthesis conditions (*i.e.* 1.5 HF, 130 °C, sample A). When the heating temperature is too high (170 °C, sample B), TMP–GaPO co-crystallizes as an impurity. In the same way, an increase in the initial amount of fluoride (3HF, sample C), leads to the crystallization of TMP–GaPO as a single phase, which is known to have a high fluoride content.[17] Finally, for a low initial amount of fluoride (1 HF), the crystallization of Mu-15 is also hampered and the product obtained at high temperature (170 °C) corresponds to $GaPO_4$–C4[24] (sample D), whereas at a lower temperature (130 °C) the recovered product is still mainly amorphous (sample E).

The SEM micrograph of the pure Mu-15 material (sample A) is shown in Fig. 1. The crystals display a needle-like morphology, with sizes ranging from 10–20 μm × 1–2 μm. Several experiments were performed in order to increase the crystal size (by increasing the water content or the viscosity of the starting mixture), but all these attempts were unsuccessful.

### 3.2 Chemical and thermal analyses

According to the elemental and thermal analyses, the as-synthesized Mu-15 sample (sample A) has the following composition (wt%): Ga, 32.8 : P, 14.2 : F, 3.2–3.4 : N, 3.4 : C, 10.1 : $H_2O$, 3.2 (resulting from adsorbed water and dehydroxylation reactions). The C/N molar ratio, close to 3.5, as in the pure TMP molecule, shows that the template is occluded intact in the structure. The Ga/P molar ratio is close to 1 and corresponds to the value usually obtained for this type of material.

The results of these analyses are in good agreement with the unit cell formula found by the structure analysis: $[Ga_{16}P_{16}O_{60}(OH)_2F_6O_4][H_2TMP]_4$. In this formula, the amine is supposed to be doubly protonated (see section 3.3).

The thermal stability under air of Mu-15 was investigated using high-temperature XRD analysis and TG/DTA thermal analysis. The TG and DTA curves of the as-synthesized Mu-15 sample are given in Fig. 2. The total weight loss, close to 22%, occurs mainly in two steps. The first (3.2 wt%), before 300 °C, corresponds to the removal of the adsorbed water combined

**Table 3** Recording conditions of the MAS and CP MAS NMR spectra for Mu-15

| | $^{19}F$ | $^{13}C$ | $^{71}Ga$ | $^{1}H$-decoupled $^{31}P$ MAS |
|---|---|---|---|---|
| Chemical shift standard | $CFCl_3$ | TMS | $Ga(H_2O)_6^{3+}$ | 85% $H_3PO_4$ |
| Frequency/MHz | 376.5 | 75.47 | 112.03 | 161.98 |
| Pulse width/μs | 3 | 6.5 | 0.7 | 3 |
| Flip angle | π/2 | π/2 | π/12 | π/2 |
| Contact time/ms | — | 2 | — | — |
| Recycle time/s | 20 | 4 | 0.5 | 8 |
| Spinning rate/Hz | 10 000 | 5000 | 10 000 | 8000 |
| Number of scans | 24 | 1450 | 106 800 | 56 |

**Table 4** Crystallographic parameters for the structure analysis of the fluorogallophospahte Mu-15

| | |
|---|---|
| Data collection | |
| Diffractometer | STOE STADI-P, Debye–Scherrer mode, with PSD |
| Sample holder | 0.3 mm glass capillary |
| Wavelength | Cu-K$\alpha_1$ |
| $2\theta$ range/° | 9.0–90.0 |
| Step size ($2\theta$)/° | 0.02 |
| Time per step/s | 3200 |
| Refinement | |
| Unit cell formula | $[Ga_{16}P_{16}O_{60}(OH)_2F_6O_4][H_2TMP]_4$ |
| Space group | $Pna2_1$ |
| $a$/Å | 16.5779(2) |
| $b$/Å | 9.8223(1) |
| $c$/Å | 13.8562(2) |
| $V$/Å$^3$ | 2256.25(6) |
| $Z$ | 1 |
| No. of observations | 4125 |
| No. of contributing reflections | 960 |
| No. of structural parameters | 73 |
| No. of profile parameters | 9 |
| $^aR_{exp}$ | 0.020 |
| $^awR_p$ | 0.033 |
| $^aR_p$ | 0.026 |
| $^aR_F$ | 0.040 |
| $^aR_F^2$ | 0.063 |
| $^a\chi^2$ | 2.70 |

[a]The definition of these parameters is given in ref. 23.

with the dehydroxylation of the Ga–OH groups or the removal of HF. It leads to a very broad endothermic peak on the DTA curve. The second (18.8 wt%), which corresponds to a series of exothermic peaks, ranging from 350 to 600 °C, is due to the decomposition of the organic species occluded in the structure (15.7 wt% according to the chemical analysis) and the removal of HF and/or the dehydroxylation of the Ga–OH groups. According to the high-temperature XRD results, this decomposition leads to an amorphisation of the structure. A cristobalite-type gallophosphate material crystallizes after heating above 600 °C.

### 3.3 $^{13}$C NMR spectroscopy

The $^{13}$C CP MAS NMR spectrum of the pure as-prepared Mu-15 sample displays 3 main groups of resonances (Fig. 3a), showing that the TMP molecule is intact. The first group consists of two peaks located at 54.8 and 52.6 ppm. They correspond to the two –$CH_2$–N groups of the TMP molecule [C(1) and C(3) atoms]. The four signals at 48.2, 46.1, 44.2 and 43.3 ppm can be assigned to the carbon atoms of the methyl groups, which are crystallographically inequivalent. Finally,

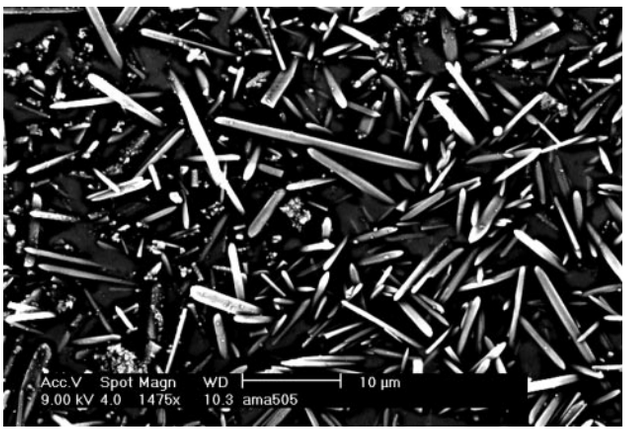


**Fig. 1** Scanning electron micrograph of the gallophosphate Mu-15 showing the needle-like morphology of the crystals.

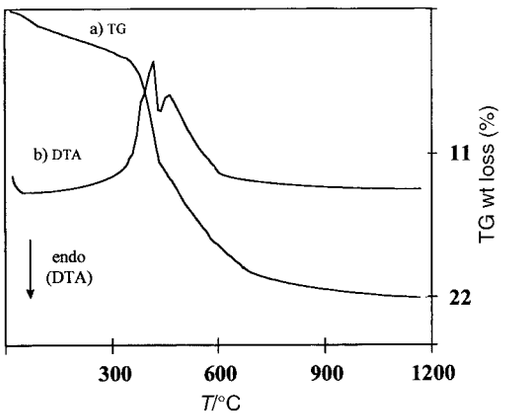


**Fig. 2** Thermal analysis of the gallophosphate Mu-15, (a) TG under air, (b) DTA under air.

the last peak observed at 21.7 ppm corresponds to the C(2) atom of the organic molecule.

These chemical shifts are closer to those observed, by $^{13}$C liquid NMR spectroscopy, for pure TMP in acid medium [pH ≈ 4, $\delta(CH_2) = 20.5$, $\delta(CH_3) = 43.5$ and $\delta(CH_2$–N) = 54.7 ppm; Fig. 3b] than in basic medium [pH ≈ 11, $\delta(CH_2) = 24.7$, $\delta(CH_3) = 44.5$ and $\delta(CH_2$–N) = 57.1 ppm; Fig. 3c]. As the two amine functions are probably protonated at acid pH, we can reasonably suppose that the organic molecule is occluded in the structure of Mu-15 in its protonated form, thus compensating the negative charge of the fluoride anions and hydroxyl groups (see chemical composition).

### 3.4 $^{19}$F NMR spectroscopy

In the $^{19}$F MAS NMR spectrum of Mu-15, the main signals are observed at −69.0 and −181.8 ppm (Fig. 4). The former, at low field, is characteristic of $F^-$ anions occluded in D4R

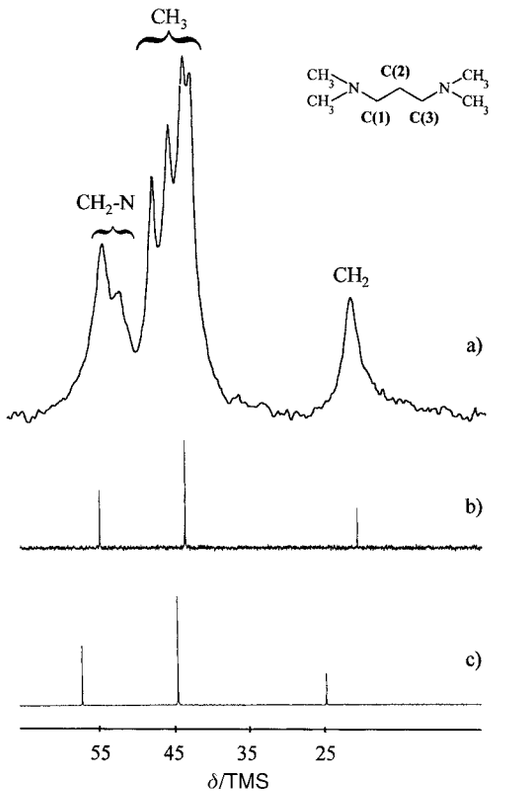


**Fig. 3** (a) $^{13}$C CP MAS NMR spectrum of the gallophosphate Mu-15, (b) $^{13}$C liquid NMR spectra of *N*,*N*,*N*′,*N*′-tetramethyl-1,3-propanediamine in acid (pH ≈ 4) and (c) basic (pH ≈ 11) aqueous solution.

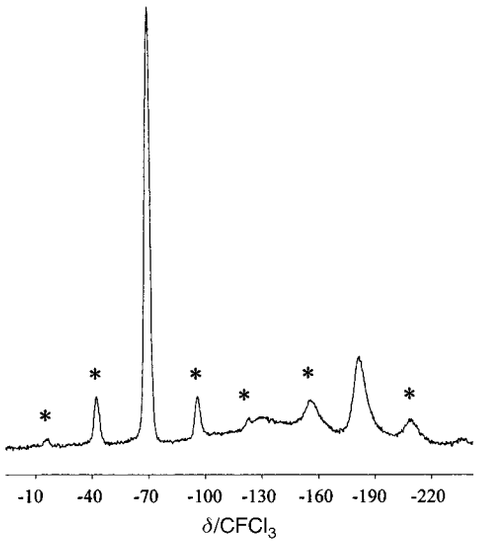


**Fig. 4** $^{19}$F MAS NMR spectrum of the gallophosphate Mu-15 (* indicates spinning side bands).

units.[4,5,12,13] As previously observed for the gallophosphate Mu-3,[13] the second resonance, at −181.8 ppm, corresponds to terminal $F^-$ ions. After deconvolution of the spectrum, the intensity ratio F(D4R)/F(Ga–F) is about 2 : 1.

### 3.5 $^{71}$Ga NMR spectroscopy

As for many other gallophosphates, the $^{71}$Ga MAS NMR spectrum of Mu-15 (Fig. 5) is poorly resolved. This is due to the strong quadrupolar effect of the gallium. Nevertheless, observing the spectrum closely, two types of environment for the Ga atoms can be distinguished, the former at 66 ppm [reference $Ga(H_2O)_6^{3+}$] and the latter at a higher field (−54 ppm). According to the structure determination (see section 3.7), these two signals might correspond to the two types of gallium atoms in 5-fold coordination: one with four oxygen and one fluorine atoms, the other with three oxygens and two fluorines or one fluorine and one hydroxyl group.

### 3.6 $^{31}$P NMR spectroscopy

The $^{31}$P MAS and CP MAS NMR spectra of Mu-15 are very similar. As an example, the $^1$H-decoupled $^{31}$P MAS NMR spectrum, given in Fig. 6, displays four different signals with the following chemical shifts: −7.1, −7.9, −12.1 and −14.7 ppm. The intensity ratio is close to 1 : 1 : 1 : 1. For

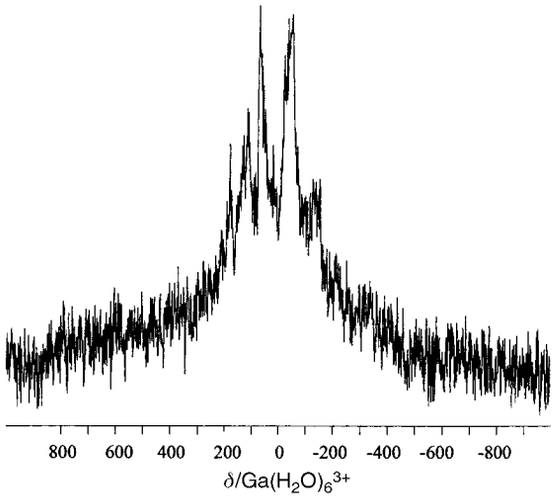


**Fig. 5** $^{71}$Ga MAS NMR spectrum of the gallophosphate Mu-15.

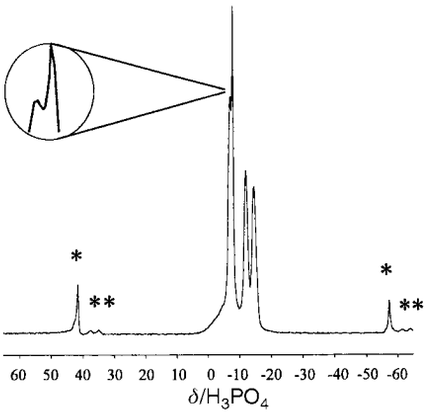


**Fig. 6** $^1$H-decoupled $^{31}$P MAS NMR spectrum of the gallophosphate Mu-15 (* indicates spinning side bands).

microporous gallophosphates, chemical shift values ranging from −10 to −20 ppm (reference 85% $H_3PO_4$) correspond generally to $Q^4$ groups [$P(OGa)_4$)], whereas values close to −5 ppm are usually assigned to $Q^3$ groups [$HO–P(OGa)_3$]. Consequently, the three resonances at −7.9, −12.1 and −14.7 ppm can be attributed to $Q^4$ groups. Moreover, whatever the contact time, no significant differences are observed between the MAS and CP MAS spectra, which indicates, in agreement with the structure determination, that no terminal P–OH groups are present. These four signals correspond to the four distinct crystallographic phosphorus sites (see section 3.7).

### 3.7 Structure determination and refinement

The X-ray powder pattern was first indexed in orthorhombic symmetry with the following unit cell parameters: $a = 16.57$, $b = 13.85$, $c = 9.82$ Å. The analysis of systematically extinct reflections indicated that a possible space group could be *Pnma*, and thus, this centrosymmetric space group was retained at first. From the whole of the experimental results given above, the idealized unit cell chemical composition of Mu-15 is $[Ga_{16}P_{16}O_{60}(OH)_2F_6O_4][H_2TMP]_4$. The structure of Mu-15 was solved in a straightforward process by direct methods (EXPO) applied to the integrated intensities as extracted from the X-ray powder data (EXTRA). The calculated Fourier map revealed a large part of the structure, *i.e.* framework atoms and the non-connected fluorine atom. In this way, three distinct crystallographic phosphorus and gallium sites were found, one at a general position (multiplicity 8) and two at a special

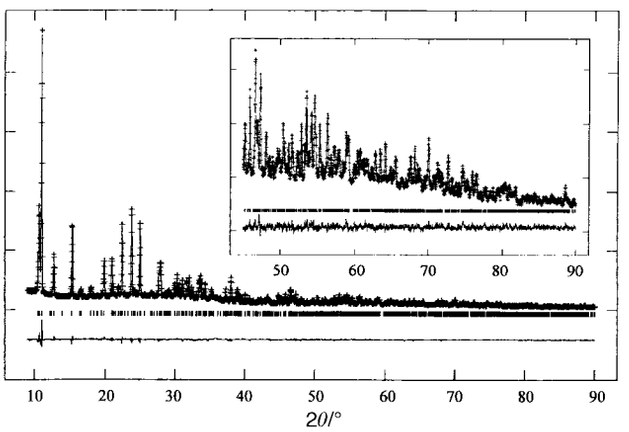


**Fig. 7** Experimental (+) and simulated (solid line) XRD patterns of the gallophosphate Mu-15. Vertical lines indicate the positions of the allowed reflections for space group $Pna2_1$. The lowest trace is the difference plot. The inset presents the high-angle part of the powder pattern, which has been expanded to show more details.

**Table 5** Atomic coordinates, isotropic displacement parameters $U_i$ (Å$^2$) and site occupancy factors (sof) for Mu-15, standard deviations are given in parentheses

| Atoms | *X* | *Y* | *Z* | $U_i \times 100$ | sof |
|---|---|---|---|---|---|
| Ga1 | 0.2734(6) | 0.1054(1) | −0.1144(2) | 1.78(4)[a] | 1 |
| Ga2 | 0.1069(2) | 0.3229(4) | −0.2505(2) | 1.78(4)[a] | 1 |
| Ga3 | −0.1617(2) | 0.0569(4) | −0.2490(2) | 1.78(4)[a] | 1 |
| Ga4 | 0.2712(6) | 0.1065(1) | −0.3933(2) | 1.78(4)[a] | 1 |
| P1 | 0.1386(4) | 0.0138(6) | −0.2519(3) | 2.42(3)[a] | 1 |
| P2 | −0.0847(4) | 0.3432(7) | −0.2472(4) | 2.42(3)[a] | 1 |
| P3 | 0.2224(7) | 0.4063(2) | −0.4219(3) | 2.42(3)[a] | 1 |
| P4 | 0.2150(7) | 0.4042(1) | −0.0816(2) | 2.42(3)[a] | 1 |
| O1 | 0.2350(2) | 0.2607(5) | −0.4567(6) | 2.23(7)[a] | 1 |
| O2 | 0.0901(8) | 0.1454(4) | −0.2405(7) | 2.23(7)[a] | 1 |
| O3 | 0.0038(1) | 0.3895(1) | −0.2523(3) | 2.23(7)[a] | 1 |
| O4 | 0.1529(2) | 0.4124(2) | −0.3522(2) | 2.23(7)[a] | 1 |
| O5 | −0.1280(1) | 0.4186(7) | −0.1691(2) | 2.23(7)[a] | 1 |
| O6 | 0.2035(3) | 0.4970(2) | −0.5076(5) | 2.23(7)[a] | 1 |
| O7 | −0.2289(1) | 0.0144(2) | −0.1473(5) | 2.23(7)[a] | 1 |
| O8 | 0.1939(2) | −0.0035(2) | −0.1649(7) | 2.23(7)[a] | 1 |
| O9 | −0.0878(8) | 0.1932(6) | −0.2249(6) | 2.23(7)[a] | 1 |
| O10 | 0.1355(1) | 0.3814(2) | −0.1314(2) | 2.23(7)[a] | 1 |
| O11 | 0.1883(2) | 0.0200(2) | −0.3416(6) | 2.23(7)[a] | 1 |
| O12 | 0.3730(2) | 0.1287(6) | −0.3437(6) | 2.23(7)[a] | 1 |
| O13 | 0.2984(1) | 0.4558(2) | −0.3725(4) | 2.23(7)[a] | 1 |
| O14 | 0.2989(2) | −0.0170(1) | −0.4903(6) | 2.23(7)[a] | 1 |
| O15 | 0.2533(2) | 0.2710(7) | −0.0572(5) | 2.23(7)[a] | 1 |
| F1 | 0.2480(2) | 0.2459(6) | −0.2595(8) | 2.1(5)[a] | 1 |
| O16 | 0.0836(8) | −0.0999(5) | −0.2582(8) | 1.81(6) | 1 |
| F2[b] | −0.0928(8) | −0.0903(4) | −0.2329(2) | 2.2(7) | 1 |
| N1 | 0.5034(6) | 0.7325(5) | −0.4245(7) | 15.2(5)[a] | 1.14[c] |
| N2 | 0.4773(4) | 0.2905(2) | −0.6050(8) | 15.2(5)[a] | 1.14[c] |
| C1 | 0.4554(4) | 0.6347(5) | −0.4821(2) | 15.2(5)[a] | 1.33[c] |
| C2 | 0.5024(9) | 0.5088(4) | −0.5136(3) | 15.2(5)[a] | 1.33[c] |
| C3 | 0.4457(6) | 0.3964(7) | −0.5379(3) | 15.2(5)[a] | 1.33[c] |
| C4 | 0.4496(2) | 0.8402(3) | −0.3798(6) | 15.2(5)[a] | 1.5[c] |
| C5 | 0.5727(7) | 0.7926(2) | −0.4789(2) | 15.2(5)[a] | 1.5[c] |
| C6 | 0.5594(5) | 0.2375(6) | −0.5794(2) | 15.2(5)[a] | 1.5[c] |
| C7 | 0.4182(7) | 0.1759(3) | −0.6155(1) | 15.2(5)[a] | 1.5[c] |

[a]Parameters with the same superscript were constrained to be equal. [b]F2 is a mixed F/OH position and was refined using half occupancies of F and O. [c]The site occupancy factors were adjusted to reflect the contribution of the H atoms to the scattering.

position (multiplicity 4). Due to the fact that the atomic position of the *N*,*N*,*N*′,*N*′-tetramethyl-1,3-propanediammonium cation was not revealed by direct methods and that the solid state $^{13}$C NMR spectrum (Fig. 3) did not show any presence of a symmetry element, its only place could be at a general position with a site occupancy factor of 0.5. The diammonium cation was placed inside the free volume of Mu-15 using the conformation given by Robertson *et al.*[25] An energy minimization performed with the Cerius2 software[26] was used for a better location. For that, the organic species was defined as a rigid body and the framework atoms fixed. This system gave the starting model for the Rietveld analysis. During the Rietveld refinement, restraints on the bond lengths and angles of the framework atoms were applied and an adequate set of soft constrains to transform the organic cation to a pseudo-rigid body was defined. At the end of the refinement, the reliability factors converged to $R_p = 0.076$ and $wR_p = 0.125$. These values are quite high and the structure is not exactly consistent with the solid state $^{31}$P NMR spectrum of the as-prepared Mu-15 which unambiguously shows four distinct peaks of the same intensity (see Fig. 6).

For this reason, and despite the fact that the powder second-harmonic generation (PSHG) measurements were negative, the refinement was performed in a non-centrosymmetric subgroup $Pn2_1a$. In order to work with the conventional space group ($Pna2_1$), an ($a\bar{c}b$) rotation of the axis was necessary and consequently an adequate matrix was applied to the atomic coordinates found in the centrosymmetric *Pnma* space group. Afterwards the missing atoms were added to complete the framework (1 gallium, 1 phosphorus and 6 oxygen atoms). At the end of the Rietveld refinement the reliability factors converged to much better values. Further details of the crystallographic data are given in Table 4. The profile fit is given in Fig. 7. Atomic coordinates, displacement parameters and site occupation factors are given in Table 5. Selected bond lengths and angles are reported in Table 6.

### 3.8 Structure description

The framework of Mu-15 can be built completely from D4R ($Ga_4P_4O_{12}$) units, which are the fundamental building blocks of the structure. It is closely related to the structures of the gallophosphates Mu-2[12] and Mu-5[14] and differs only by the connection scheme of the D4Rs.

As observed for these two gallophosphate materials, all the D4R units contain a fluoride anion inside. Each unit is interconnected with six other building blocks *via* common oxygen atoms. The remaining two corners of the D4R are P=O (or P–O$^-$, see below) and Ga–F/OH (see Table 5 and Fig. 8). The structure consists of layers of D4Rs parallel to the (*b*,*c*) plane, showing 10-ring openings. Such layers are linked to each other to form a three dimensional framework with two types of channel systems: the first, delimited by 10-MR, runs along the [100] direction (Fig. 9), whereas the other, parallel to the [010] direction, is delimited by 8-ring apertures (Fig. 10).

The fluorine atom F1 is occluded in the D4R unit, whereas F2 is a terminal ion (F$^-$ or OH$^-$, see Table 5 and Fig. 8). All the gallium atoms are in 5-fold coordination with a trigonal bipyramidal geometry, but do not display exactly the same environment. Ga1, Ga2 and Ga4 are coordinated to four framework oxygen atoms [1.77(2) Å $< d$(Ga–O) $<$ 1.87(2) Å] and the fluorine occluded in the D4Rs [2.34(4) Å $< d$(Ga–F) $<$ 2.48(4) Å], whereas Ga3 is coordinated to three framework oxygen atoms [1.84(2) $< d$(Ga–O) $<$ 1.85(1) Å], the

**Table 6** Selected interatomic distances (Å) and bond angles (°) in the structure of Mu-15, standard deviations are given in parentheses

| Atoms | Distances/Å | Atoms | Distances/Å |
|---|---|---|---|
| Ga1–O5 | 1.82(2) | Ga3–O7 | 1.84(2) |
| Ga1–O6 | 1.86(2) | Ga3–O9 | 1.85(1) |
| Ga1–O8 | 1.84(2) | Ga3–O13 | 1.84(2) |
| Ga1–O15 | 1.84(2) | Ga3–F1 | 2.45(2) |
| Ga1–F1 | 2.48(4) | Ga3–F2 | 1.86(1) |
| Ga2–O2 | 1.77(1) | Ga4–O1 | 1.85(2) |
| Ga2–O3 | 1.83(1) | Ga4–O11 | 1.77(2) |
| Ga2–O4 | 1.83(2) | Ga4–O12 | 1.83(2) |
| Ga2–O10 | 1.81(2) | Ga4–O14 | 1.87(2) |
| Ga2–F1 | 2.46(2) | Ga4–F1 | 2.34(4) |
| **Atoms** | **Angles/°** | **Atoms** | **Angles/°** |
| O5–Ga1–O6 | 94.1(9) | O7–Ga3–O9 | 115.3(8) |
| O5–Ga1–O8 | 114.3(9) | O7–Ga3–O13 | 118.6(7) |
| O5–Ga1–O15 | 117.2(8) | O7–Ga3–F1 | 81.7(11) |
| O5–Ga1–F1 | 83.5(9) | O7–Ga3–F2 | 96.0(8) |
| O6–Ga1–O8 | 96.7(9) | O9–Ga3–O13 | 117.1(8) |
| O6–Ga1–O15 | 101.6(8) | O9–Ga3–F1 | 81.0(7) |
| O6–Ga1–F1 | 177.6(10) | O9–Ga3–F2 | 97.7(6) |
| O8–Ga1–O15 | 123.3(8) | O13–Ga3–F1 | 77.2(11) |
| O8–Ga1–F1 | 83.9(10) | O13–Ga3–F2 | 106.3(9) |
| O15–Ga1–F1 | 80.0(10) | F1–Ga3–F2 | 176.5(14) |
| O2–Ga2–O3 | 101.8(6) | O1–Ga4–O11 | 109.5(8) |
| O2–Ga2–O4 | 126.9(8) | O1–Ga4–O12 | 112.3(8) |
| O2–Ga2–O10 | 106.4(8) | O1–Ga4–O14 | 105.6(8) |
| O2–Ga2–F1 | 81.5(6) | O1–Ga4–F1 | 81.0(10) |
| O3–Ga2–O4 | 102.0(10) | O11–Ga4–O12 | 128.4(9) |
| O3–Ga2–O10 | 98.2(10) | O11–Ga4–O14 | 99.8(8) |
| O3–Ga2–F1 | 175.3(12) | O11–Ga4–F1 | 80.4(10) |
| O4–Ga2–O10 | 116.2(6) | O12–Ga4–O14 | 96.9(8) |
| O4–Ga2–F1 | 73.3(11) | O12–Ga4–F1 | 77.6(9) |
| O10–Ga2–F1 | 84.0(12) | O14–Ga4–F1 | 172.8(10) |
| O–P–O | minimum 108.7(4)° | | |
| | maximum 110.2(4)° | | |
| | average 109.5° | | |

trapped fluoride ion F1 [$d$(Ga–F1) = 2.45(2) Å] and a terminal anion F2 [$F^-$ or $OH^-$, see Table 5, $d$(Ga–F2) = 1.86(1) Å]. This might explain the two main signals observed in the $^{71}$Ga MAS NMR spectrum (Fig. 5).

All the phosphorus atoms are in 4-fold coordination with oxygen atoms and are not affected by the presence of the fluoride ion trapped in the D4R units [$d$(P–F1) = 2.78(4) Å] so that they all adopt an almost perfect tetrahedral environment (average O–P–O angle = 109.5°). P2, P3 and P4 correspond to phosphorus only connected to gallium atoms *via* four oxygens [1.49(1) Å < $d$(P–O) < 1.54(1) Å], whereas P1 is connected to three gallium atoms and one oxygen atom. It should be noticed that it is difficult to distinguish between a P=O (or a $P–O^-$) and a P–OH group from powder data. Nevertheless, the distance

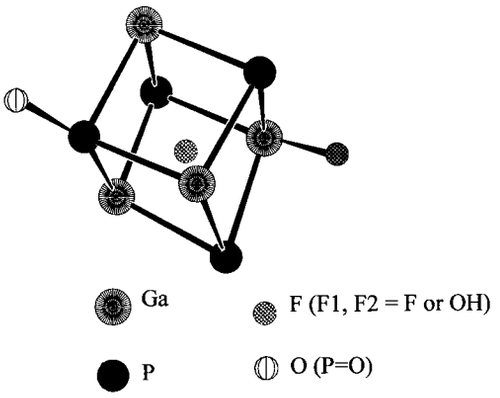


**Fig. 8** Scheme of the D4R unit hosting $F^-$: the fundamental building block of the structure of Mu-15.

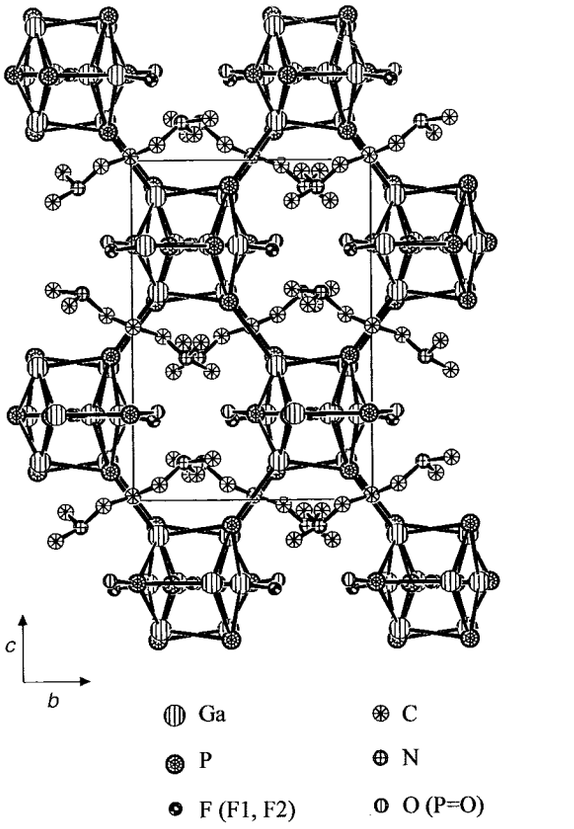


**Fig. 9** Projection of the structure of Mu-15 along the [100] direction showing the 10-membered ring openings (for clarity, the oxygen bridges are omitted).

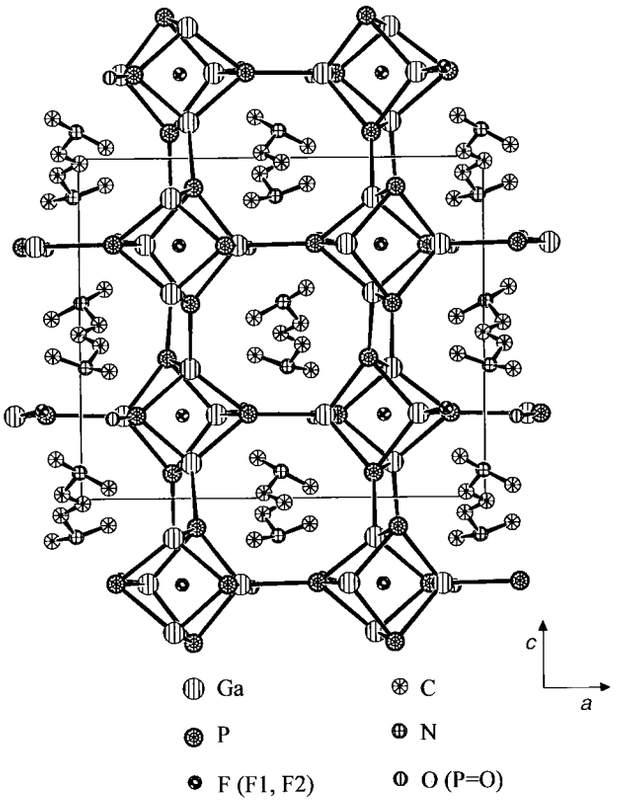


**Fig. 10** Projection of the structure of Mu-15 along the [010] direction showing the 8-membered ring channels (for clarity, the oxygen bridges are omitted).

P1–O16 is very short [1.44(1) Å] and fits better with a P=O than a P–OH (expected bond length ≈ 1.56 Å).[27] Moreover, according to the chemical analysis (neutrality of the compound) and the $^{31}$P MAS NMR spectroscopy (no significant difference observed between the MAS and CP MAS spectra, whatever the contact time), the absence of a P–OH group seems to be confirmed.

The structure reveals short contacts between the organic cation (*N*,*N*,*N*′,*N*′-tetramethyl-1,3-propanediammonium) and the oxygen atoms of the framework. The shortest distances are N1···O = 2.96(3), N2···O = 2.58(3) and N1···F2(F/OH) = 3.40(3), N2···F2(F/OH) = 2.86(3) Å. These interactions are somewhat hydrogen bonding in nature.

## 4 Conclusion

Mu-15 was obtained in the presence of *N*,*N*,*N*′,*N*′-tetramethyl-1,3-propanediamine (TMP) as organic template. The fact that it crystallizes with the same structure-directing agent as that used to prepare TMP-GaPO,[17] constitutes further proof of the wide reactivity of the gallophosphate system.

The structure of this new gallophosphate is closely related to the structures of Mu-2[12] and Mu-5.[14] All these materials result from the connection of fluorinated D4R units. The structure of Mu-15 differs from the two other fluorogallophosphates by the connection scheme of these units.

This new fluorogallophosphate is another example showing the very specific effect of the fluoride anion for stabilizing the D4R units. It should be noted that, at the present time, in the gallophosphate system, such units have never been obtained in the absence of fluoride anion.

## Acknowledgements

The authors would like to thank "Institut Français du Pétrole" (IFP) which kindly provided the gallium nitrate source. Thanks are also due to Dr A. Ibanez from the Laboratoire de Cristallographie of Grenoble for the PSHG measurements.

## References

1 R. M. Barrer, *Hydrothermal Chemistry of Zeolites*, Academic Press, London, 1982.
2 S. T. Wilson, B. M. Lock and E. M. Flanigen, *US Patent*, 4310440, 1982.
3 J. B. Parise, *J. Chem. Soc., Chem. Commun.*, 1985, 606.
4 M. Estermann, L. B. McCusker, Ch. Baerlocher, A. Merrouche and H. Kessler, *Nature*, 1991, **352**, 320.
5 A. Simmen, J. Patarin and Ch. Baerlocher, in *Proceedings of the 9th International Zeolite Conference, Montreal, 1992*, ed. R. Von Ballmoos, J. B. Higgins and M. M. J. Treacy, Butterworth-Heinemann, Stoneham, MA, 1993, vol. I, p. 433.
6 F. Taulelle, A. Samoson, T. Loiseau and G. Férey, *J. Phys. Chem. B*, 1998, **102**, 8588.
7 T. Loiseau and G. Férey, *J. Solid State Chem.*, 1994, **111**, 407.
8 C. Schott-Darie, H. Kessler, M. Soulard, V. Gramlich and E. Benazzi, in *Zeolites and Related Microporous Materials: State of the Art 1994, Studies in Surface Science and Catalysis*, ed. J. Weitkamp, H. G. Kaige, H. Pfeifer and W. Hölderich, Elsevier, Amsterdam, 1994, p. 101.
9 A. Meden, R. W. Grosse-Kunsleve, Ch. Baerlocher and L. B. McCusker, *Z. Kristallogr.*, 1997, **212**, 801.
10 G. Férey, T. Loiseau, P. Lacorre and F. Taulelle, *J. Solid State Chem.*, 1993, **105**, 179.
11 S. Kallus, J. Patarin and B. Marler, *Microporous Mater.*, 1996, **7**, 89.
12 P. Reinert, B. Marler and J. Patarin, *Chem. Commun.*, 1998, 1769.
13 P. Reinert, J. Patarin, T. Loiseau, G. Férey and H. Kessler, *Microporous Mesoporous Mater.*, 1998, **22**, 43.
14 T. Wessels, L. B. McCusker, Ch. Baerlocher, P. Reinert and J. Patarin, *Microporous Mesoporous Mater.*, 1993, **23**, 67.
15 A. M. Chippindale, R. I. Walton and C. Turner, *J. Chem. Soc., Chem. Commun.*, 1995, 1261.
16 P. Reinert, B. Marler and J. Patarin, *Microporous Mesoporous Mater.*, 2000, in press.
17 S. J. Weigel, T. Loiseau, G. Férey, V. Munch, F. Taulelle, R. E. Morris, G. D. Stucky and A. K. Cheetham, in *Proceedings of the 12th International Zeolite Conference*, M. M. J. Treacy, B. K. Marcus, M. E. Bisher and J. B. Higgins, Material Research Society, 1999, vol. IV, p. 2453.
18 P. E. Werner, L. Eriksson and M. Westdhal, *J. Appl. Crystallogr.*, 1985, **18**, 367.
19 A. Altomare, M. C. Burla, G. Cascarano, C. Giacovazzo, A. Guagliardi, A. G. G. Moliterni and G. Polidori, *J. Appl. Crystallogr.*, 1995, **28**, 842.
20 A. Altomare, G. Cascarano, C. Giacovazzo, A. Guagliardi, M. C. Burla, G. Polidori and M. Camalli, *J. Appl. Crystallogr.*, 1994, **27**, 435.
21 A. Le Bail, H. Duroy and J. Fourquet, *Mater. Res. Bull.*, 1988, **238**, 447.
22 G. Cascarano, L. Favia and C. Giacovazzo, *J. Appl. Crystallogr.*, 1992, **25**, 267.
23 A. C. Larson and R. B. Von Dreele, LANSCE, MS-H 805, Los Alamos National Laboratory, 1995.
24 S. Feng and R. Xu, *Chem. J. Chin. Univ. (Engl. Edn.)*, 1988, **4**, 1.
25 K. N. Robertson, T. S. Cameron and O. Knop, *Can. J. Chem.*, 1996, **746**, 1572.
26 Cerius2® Version 3.8, Biosym/Molecular Simulations, Cambridge, UK, 1998.
27 P. Reinert, N. Zabukovec Logar, J. Patarin and V. Kaucic, *Eur. J. Solid State Inorg. Chem.*, 1998, **35**, 373.